PPPL-2010

UC20-F

I-9934

MASTER

PPPL--2010

DE83 013722

PPPL-2010

Dr. 1529-6

CONF-820944--9

X-RAY ANALYSIS OF NONMAXWELLIAN DISTRIBUTIONS (CURRENT DRIVE)

By

S. von Goeler, J. Stevens, W. Stodiek, S. Bernabei, M. Bitter, T.K. Chu, K.W. Hill, D. Hillis, W. Hooke, F. Jobes, G. Lenner, E. Meservey, R. Motley, N. Sauthoff S. Sesnic, and F. Tenney

JUNE 1983

PLASMA PHYSICS LABORATORY

PRINCETON UNIVERSITY

PRINCETON, NEW JERSEY

PREPARED FOR THE U.S. DEPARTMENT OF ENERGY, UNDER CONTRACT DE-AC02-76-CHO-3073.

X-RAY ANALYSIS OF NONMAXWELLIAN DISTRIBUTIONS (CURRENT DRIVE)†

S. von Goeler, J. Stevens, W. Stodiek, S. Bernabei,
M. Bitter, T.K. Chu, K.W. Hill, D. Hillis*, W. Hooke,
F. Jobes, G. Lenner, E. Meservey, R. Motley, N. Sauthoff,
S. Sesnic, and F. Tenney

Plasma Physics Laboratory, Princeton University
Princeton, New Jersey 08544

ABSTRACT

The plasma bremsstrahlung emission is utilized to determine the shape of the electron velocity distribution in situations where it deviates strongly from a Maxwellian distribution. The instrumentation used to measure the hard X-ray emission is briefly discussed. Model calculations show that polarization measurements give best results for unrelativistic tails with tail temperatures $T_h < 50$ keV, whereas measurements of the angular distribution of the x-ray emission based on the forward scattering of bremsstrahlung for relativistic electrons yields the best information for $T_h > 50$ keV. The techniques were originally developed in order to analyze runaway discharges. Recently, they found new interest because of the formation of energetic electron tails during current drive. The first x-ray results from the current [illegible] during LH heating on PLT are discussed.

---

†Presented at the Course and Workshop "Diagnostics for Fusion Reactor Conditions," Varenna (Como) Italy, September 6-17, 1982.
*On leave from Oak Ridge National Laboratory, Oak Ridge, Tennessee.

DISCLAIMER

I. INTRODUCTION

Almost all tokamak discharges produce hard X rays, and many of the emitted X-ray photons have energies in the range of several MeV. This fact indicates that there must exist a tail of energetic electrons in a tokamak plasma and that the electron-velocity distribution must be nonMaxwellian to some degree. Most of the hard X rays are produced when the energetic electrons hit the limiter or the walls of the vacuum chamber. However, some small fraction of the X-ray emission is produced in electron collisions with the ions of the plasma. By careful experimentation the resulting plasma bremsstrahlung can actually be measured, and the X-ray data can be utilized to analyze the velocity distribution of the energetic electron tail.

On the pioneering tokamaks like the Soviet TM3 and T3 or Princeton's ST, the hard X-ray tail was a prominent feature.[1] Some typical X-ray spectra from the ST tokamak are shown in Fig. 1. The parameter for the various curves is the neutral-gas filling pressure, which determines the plasma density. On ST all low density discharges ($n_e < 2.5 \times 10^{13}$ cm^{-3}) exhibited a strong tail with a slope corresponding to approximately 100 keV. Sometimes an additional component with intermediate slope of 10-20 keV appeared at lower energies. Some of the intermediate tails could be attributed to transients in the X-ray emission. On ST, there was only a relatively small operating range at high density (5×10^{13} cm$^{-3} < n_{eo} < 1 \times 10^{14}$ cm^{-3}) where the discharge had a purely thermal Maxwellian velocity distribution.

On the larger tokamaks that have followed the pioneering machines, for instance on T10 or PLT, hard X-ray tails are prominent only at low plasma densities ($n_e < 1 \times 10^{13}$ cm^{-3}), and the investigation of the high energy bremsstrahlung lost its urgency. A sudden change of interest occurred, however, about a year ago, when large scale current drive was demonstrated on

PLT by the lower hybrid (LH) heating group under W. Hooke.[2] A few months later it was shown that the current drive is connected to the formation of a hot electron tail, and at present, a vigorous program for studying the energetic electrons is being carried out on PLT.

It is the purpose of this paper to describe the experimental techniques which are used for the X-ray analysis of energetic electrons. We shall give a brief description of the instrumentation in Sec. I. In Sec. II, we will discuss how the X-ray emission is related to the electron-velocity-distribution function, i.e., we shall talk about bremsstrahlung production. In particular, we want to discuss techniques for determining electron-velocity components parallel and perpendicular to a magnetic field. As an illustration of the application of these techniques we will review in Sec. III some older measurements from ST of electron runaway formation. In Sec IV we present the very recent X-ray results on the LH-current drive in PLT. It should be pointed out that the hard X-ray techniques were originally developed for magnetic mirrors in order to diagnose the hot electron rings generated in electron-cyclotron-heated plasmas.[3-5]

I. INSTRUMENTATION

A layout of the hard X-ray detector for the current drive experiment on PLT is shown in Fig. 2. The X-ray photons are detected by a NaI(Tl) scintillator-photomultiplier combination. A detailed discussion of the properties of sodium iodide detectors was given in the 1978 Varenna lecture of H. Knoepfel[6] and, therefore, is not repeated here. In order to increase the photopeak efficiency and reduce the Compton tail,[7] the scintillators should be large enough to reabsorb the Compton-scattered photons. We prefer 3" × 3" NaI crystals which have practically 100% photopeak efficiency up to 1 MeV. Larger

crystals have been used; they require, however, a very large amount of shielding to keep out cosmic rays, hard X rays from the limiter, and γ rays resulting from (n,γ) reactions produced by fusion neutrons. The 3" x 3" detector in Fig. 2 is shielded by 4 in. of lead and 20 cm of borated polyethylene. Relatively few neutrons (< 10^8 per sec.) are formed in the current-drive regime ($n_e < 10^{13}$ cm^{-3}). However they are generated slightly above the high density limit of the current drive on PLT at a rate of approximately 10^{11} per sec. The photomultiplier is shielded against stray magnetic fields from the OH transformer by a soft iron pipe and μ-metal foils. Another problem area is created by radiation from the wall of the vacuum vessel. In order to eliminate wall radiation, the 0.010" -Beryllium windows of the PLT system are mounted and recessed on 45-cm long steel pipes. The optical path of the system is carefully aligned by a set of lead apertures so that the detector can view only the beryllium window, but not the flange on which the beryllium is mounted or the steel pipe. For some applications it is impossible to provide these precautionary measures. It then may be possible to reduce wall bombardment and therefore radiation by increasing the distance between the limiter and the vacuum-vessel wall.

II. BREMSSTRAHLUNG EMISSION

X-ray continua are produced by bremsstrahlung and recombination radiation. For thermal emission, the recombination radiation tends to be more important by a factor of approximately 2 to 10. However, since the bremsstrahlung emission is proportional to the square root of the temperature, while recombination radiation scales like $T_e^{-1/2}$, the high energy tails of the X-ray radiation tend to be produced predominantly by bremsstrahlung. We shall consequently concentrate on the bremsstrahlung.

We start our discussion by presenting three very simple physical models which are helpful for the understanding of bremsstrahlung:

(a) Kramer's rule: This model provides a crude answer to the question of how many photons an electron with kinetic energy T emits in the bremsstrahlung process. According to Kramer's rule the power spectrum of the emitted radiation is flat up to the photon energy k = T and has the value[8]

$$\frac{dW}{dk} = n_i v_e \, k \frac{d\sigma}{dk} = n_i v_e \frac{8\pi}{3\sqrt{3}} \frac{Z^2 r_o^2}{137} \frac{m_o c^2}{T}. \qquad (1)$$

W is the emitted power, k the photon energy, n_i the ion density, v_e the electron velocity, $r_o = e^2/m_o c^2$ the classical electron radius, m_o the electron rest mass, and Z the charge number of the ions. We have plotted Kramer's rule in Fig. 3 and have also added a few more realistic representations of the power spectrum.[9] Kramer's rule loses its validity in the relativistic region when the electron energy approaches and exceeds 2.5 MeV.[9] Formulas for relativistic bremsstrahlung have been listed in a review article by Koch and Motz.[10] Very exact cross sections for plasma physics application have been more recently calculated by Pratt.[11]

(b) Polarization: For close encounters between an electron and an ion, the attractive Coulomb force is predominantly in the direction of the initial electron motion. The bremsstrahlung near the short wavelength limit of the spectrum is therefore polarized in the direction parallel

to the initial electron velocity (Fig. 4). For distant encounters, i.e., in the limit of long wavelength, the electric field vector is predominantly perpendicular to the orbit and the radiation is polarized perpendicular to the electron direction. The polarization of the radiation disappears when the kinetic energy of the electron approaches the rest energy $m_o c^2$ and is actually inverted for still higher energies.[12]

(c) Angular distribution of bremsstrahlung: For nonrelativistic energies the X-ray emission is from a dipole in the parallel direction plus an isotropic component. For higher energies, relativistic effects and the effects associated with retarded potentials lead to emission in the forward direction. Figure 5 illustrates that the forward emission is already appreciable for energies as low as 20 keV.

In order to analyze the hot electron rings in magnetic mirror machines A. England has written a computer program that calculates the plasma-bremsstrahlung emission for a given electron-velocity-distribution function. Relativistic bremsstrahlung cross sections like the ones by Gluckstern and Hull[13] or Fronsdal and Uberall[14] have to be used for this purpose. More recent investigations of the emission from ECH heated plasmas are described in references.[15,16] At Princeton we used a similar program for analyzing the electron-velocity-distribution function in tokamaks. The output from these programs depends, of course, on the assumption made about the velocity-distribution function and is quite different for mirrors and tokamaks. In order to illustrate typical results from computer codes, we have plotted in Figs. 6, 7, and 8 bremsstrahlung for a relativistic Maxwellian

energy distribution f_M[17]

$$f_M = \frac{E\left(E^2 - 1\right)^{1/2}}{T\, G(T)} \exp\left(-\frac{E}{T}\right) \tag{2}$$

Here $E = 1 + T/(m_o c^2)$ is the relativistic energy of an electron in units of mc_o^2, $T = kT_t/m_o c^2$ is the normalized tail temperature, and G is a factor that normalizes the velocity-distribution functior to 1. The tail electrons are assumed to occupy a cone with angle θ_e in momentum space. The bremsstrahlung intensity I is computed by using the differential cross section $d\sigma$ and integrating over the cone and the energy,

$$I(\theta_d, \theta, k, T) = \text{const} \int_{\theta_e} d\Omega_e\, q(\Omega_e, E) \int_1^\infty v\, k\, \frac{d\sigma\left(\theta_k, E\right)}{d\Omega_k\, dk} f_M(E)\, dE \tag{3}$$

$$= \text{const} \int_0^{\theta_e} d\Omega_e\, q(\Omega_e, E) \int_1^\infty \left[\frac{c(E^2 - 1)^{1/2}}{E} k \frac{d\sigma}{d\Omega_k\, dk} \frac{E\,(E^2-1)^{1/2}}{T\, G(T)} \exp\left(\frac{-E}{T}\right)\right] dE\ .$$

θ_k is the angle between the electron velocity $\vec{v}$ and the direction of photon emission $\vec{k}$, $d\Omega_k$ is a solid angle element in direction of $\vec{k}$, and $d\Omega_e$ is a solid angle element of the electron cone. The function q normalizes the integration of the electron distribution function over a cone to 1. The bremsstrahlung intensity depends then on the tail temperature T, the photon energy k, and the angle θ_d between the axis of the electron cone and the viewing line of the detector and the electron cone angle θ_e.

Figure 6 shows the X-ray photon counts ($\equiv I(k)/k$) predicted for a beam of electrons ($\theta_e \approx 0.6°$) for emission perpendicular to the beam (detector angle $\theta_d = 90°$). The parameter for the curves is the tail temperature T_t (not to be confused with the kinetic energy T). Figure 7 shows the polarization of the radiation for the same conditions. The polarization of the radiation disappears as one would expect when there are too many relativistic electrons, i.e., when the tail temperature T_t exceeds 50 keV. On the other hand, forward scattering is stronger for more relativistic tails, and forward scattering is the technique to use for $T_t > 50$ keV. We shall present actual measurements of the forward scattering in the next section. The amount of X-ray emission for $\theta_d = 90°$ depends critically on how isotropic the velocity distribution is. This is illustrated in Fig. 8, where the emission from a beam at $\theta_d = 90°$ is only a tenth of that of an isotropic tail with an identical number of electrons and an identical temperature.

The X-ray analysis has found application in two areas of tokamak physics, namely, for the investigation of electron runaway tails and for the study of the lower-hybrid current drive.

III. PLASMA BREMSSTRAHLUNG FROM RUNAWAY ELECTRONS

In tokamaks, passing particles are on confined orbits, and electrons can be consequently accelerated to energies of many MeV before they are lost due to the increasing shift of their particle drift surfaces.[18] For particles with high enough energy, the friction force becomes very small and the inertial force balances acceleration by the electric field. As a first guess, one would consequently approximate the high energy part of the distribution by a free-fall distribution. In order to derive a formula for the free-fall distribution, we assume that runaways are generated by a mechanism, which is

not specified for the moment, and that they are supplied with momentum p_o at time t_o at the runaway rate $\dot{n}_R(t)$. The force K on the electron is

$$K = eE = \frac{eV_{OH}}{2\pi R} = \frac{dp}{dt} \tag{4}$$

where E is the toroidal electric field, V_{OH} the loop voltage around the torus, and R the major radius of the tokamak. Equation (4) can be integrated

$$p - p_o = \frac{e}{2\pi R} \int_{t_o}^{t} V_{OH}(t')\, dt' \quad . \tag{5}$$

If we assume that V_{OH} is known from measurements and if we keep the time point t fixed, then the momentum p of an electron is a function of t_o only. The inverse function is named h,

$$t_o = h(p) \quad . \tag{6}$$

At the time t_o and near p_o the distribution function has the value

$$f(p_o, t_o)\, dp_o = \dot{n}_R(t_o)\, dt_o$$

where dp_o and dt_o obey Eq. (4). Assuming that the particles are accelerated to higher energies by free-fall (and that nothing happens to them on their way up) we obtain

$$f(p,t) = \frac{2\pi R}{eV_{OH}(t)}\ \dot{n}_R\ [h(p)]\ . \qquad (7)$$

This is the desired formula for the free-fall distribution function. The formula shows that the distribution function reflects the time history of the runaway rate.

Let us now consider a particularly simple situation where a tokamak discharge, and in particular $\dot{n}_R$ and V_{OH}, become stationary after a short initial adjustment period. The free-fall distribution then becomes

$$\begin{aligned} f(p,t) \quad &= \text{const for } p \leq p^* \\ &= 0 \quad \text{for } p > p^* \end{aligned} \qquad (8)$$

where p^* is the momentum reached by the runaway electrons created first in the discharge. The corresponding energy, E^*, is

$$E^{*2} = p^{*2}c^2 + (m_0c^2)^2\ . \qquad (9)$$

The simplified free-fall-velocity-distribution function, Eq. (8), turns out to be a very useful tool for the experimental analysis and we therefore have calculated and display in Figs. 9a and 9b the bremsstrahlung spectra that originate from a beam of electrons with a free-fall distribution. In Fig. 9a the beam is observed by a detector at an angle of 60° from the beam direction. Spectra for 90 have a very similar shape but somewhat smaller

intensity. In Fig. 9b the beam is observed at 3° from the beam direction. There are a number of features of these graphs which merit attention:

(a) The spectra shown in Fig. 9a fall off in an approximately exponential fashion. This fact can easily lead to misinterpretation of experiments: An exponential photon spectrum does not necessarily imply an exponential velocity-distribution function.

(b) A comparison of Fig. 9b with Fig. 9a shows that the X-ray emission peaks in the forward direction, as is expected from our discussion in connection with Fig. 5. The more the parameter of the curves, E*, increases, the larger is the fraction of the radiation that goes into the forward direction.

(c) The electron distribution function with E* = 6 differs from the distribution function with E* = 5 only in that some electrons have been added in the energy interval $5 < E < 6$. As a consequence, the difference between the two photon spectra labeled E* = 5 and E* = 6 is due only to electrons in that energy interval. This special feature is very helpful in order to visualize and estimate what the contribution of a group of electrons is to the photon spectrum. It is obvious from Fig. 9c, for instance, that the tangential emission is produced predominantly by the most energetic particles. For the 60° or 90° view, the relative contribution of the very energetic particles is reduced and, therefore, the perpendicular view seems better suited for measuring the low energy portion of the distribution function.

We now want to show some experimental data, which go back to the ST tokamak,[19,20] and which represent still the most detailed application of these concepts to the tokamak. Figure 10 shows radial profiles of the hard X-ray emission from ST at a variety of times during a discharge with moderate runaway formation. Also shown is the electron temperature and the critical electric field, E_{crit}, according to Dreicer.[21] The figure shows that the runaway electrons are located in the central region of the plasma, where theory would predict that they are created.

The forward emission of the bremsstrahlung was quite pronounced for these discharges. Figure 11 shows X-ray spectra observed at ± 30° with respect to the direction of the major radius. Free-fall spectra have been fitted to the spectra and give good agreement for the cut-off parameter $E^* = 2$.

Figure 12 shows a comparison between a tangential X-ray spectrum (electrons moving towards the detector) and a spectrum measured at 60° to the magnetic axis. For comparison we have also plotted several theoretical curves. A free-fall spectrum has been fitted to the tangential spectrum. The corresponding free-fall spectrum for 60° does not include corrections for geometric effects, i.e., the reduction in line of sight for the 60° detection. The reduction depends on the radial profile of the hard X-ray emission. The radial profile was unfortunately not measured for this particular discharge. However, if we consider the data shown in Fig. 11 and assume that the hard X-rays originate from the central region ($r < 3$ to 4 cm) then this correction amounts to a factor 7 to 8. The dashed curve resulting from the free-fall distribution fits the measured 60° spectrum for large photon energies, but predicts too small an X-ray intensity at low energies. The data indicate that the free-fall distribution function $f(p) = \text{const}$ does

not provide a good representation of the experimental data, but that a monotonically decreasing function of the momentum p would be a better choice.

There is other evidence that confirms this finding. In Fig. 13 we show for instance a time sequence of three consecutive hard X-ray spectra for two discharges labelled (a) and (b). A free-fall curve has been fitted to the first spectrum measured at 14 ms. Since the loop voltage is known, one can calculate how the spectrum should develop in time using Eqs. (5) and (7). The corresponding free-fall spectra for times t = 27 ms and 40 ms are also plotted in Fig. 13. The experimental spectra at 27 and 40 ms do not seem to expand to higher energies, but rather seem to saturate. It has been proposed[20] that this behavior is caused by radial transport of runaway electrons across the magnetic field. A confinement time τ can be estimated by calculating the time that it takes for an electron to free-fall to an energy E_f^*, the value that gives a good fit for the saturated spectrum. A variety of data for the runaway confinement time τ from ST has been plotted in Fig. 13c.

According to the free-fall model (Eq. 7) the intensity of the X-ray emission should provide some indication of the runaway rate $\dot{n}_R$. Attempts have been made to measure $\dot{n}_R$ and to compare the result with theoretical predictions for the runaway rate. The comparison is shown in Fig. 14. The very early predictions by Dreicer[21] are much too high. This is also the case for the presently generally accepted theory of Kruskal and Bernstein.[22] Kulsrud and Sun[23] have tried to improve the theory by incorporating the additional friction generated by impurities, and also by incorporating a finite particle lifetime τ into the theory. They were successful in explaining the order of magnitude of experimental data. The confinement time τ for the particles seems, however, somewhat shorter than one would have expected from the discussion in connection with Fig. 13.

IV. PLASMA BREMSSTRAHLUNG DURING LOWER-HYBRID CURRENT DRIVE

A renewed interest in the techniques for analyzing plasma bremsstrahlung has occurred because of the successful demonstration of lower-hybrid current drive on PLT,[24-26] and in this section we want to discuss the first and as yet somewhat preliminary measurements of the hard X-ray emission from RF generated electron tails.

A typical PLT discharge with current drive is shown in Fig. 15. The current in the primary winding of the ohmic heating transformer is kept constant after the plasma current has reached its maximum at 300 kA. The plasma current decays from then on with an L/R decay time. With the 800 MHz lower hybrid power switched on, the current can be maintained at a level of 250 kA for very long times with no ohmic heating power transmitted to the discharge. The longest actually observed time was 3.5 sec. The plasma density for these discharges falls in the range 10^{12} cm^{-3}. For densities of $8 \cdot 10^{12}$ cm^{-3} and larger the current drive capability of the RF seems abruptly to disappear.

X-ray techniques have shown that a fast electron tail forms soon after the RF is switched on. After about 30 ms the evolution of the tail is completed and a stationary electron distribution is established provided that discharge conditions are kept constant. The X-ray tail formation is shown in Fig. 16. The X-ray spectra were recorded with lithium drifted silicon detectors before (Fig. 16A) and after (Fig. 16B) the RF was turned on. The spectrum in Fig. 16A is purely thermal with a temperature of 1.14 keV. A straight line fit to the photon-tail in Fig. 16B indicates a "tail" temperature of 29 keV. The 3-mm thick Si(Li) detectors become transparent to X rays with energies above 25 keV. More accurate information on the photon

spectrum can be obtained with the sodium iodide detector described in Sec. II. Figure 17 shows a measurement of the energetic photon tail with the 3" x 3" NaI detector. The spectrum falls almost exponentially over three orders of magnitude. A variety of theoretical curves has been fitted to the data. If we assume that the electron distribution is nearly isotropic and Maxwellian, then the photon tail shown in Fig. 17 would indicate an electron-tail temperature of ≈ 100 keV. If the electrons form a beam and their energy distribution remains Maxwellian, then the electron-tail temperature would be 150 keV. However, a relatively flat electron distribution function like the free-fall distribution, f(p) = const. can also be fitted to the data. The energy E^* would have to be 600 keV in order to match the data shown in Fig. 17. Measurements of the angular variation of the X-ray emission have to be performed to shed more light on the exact shape of the distribution function.

It has been speculated that LH current drive requires as a precondition the presence of a so-called slide away condition, i.e., the formation of a runaway tail at very low plasma density.† The X-ray measurements show, however, that there is very little tail formation before the RF is applied (Fig. 16), and that in the absence of RF, there is no tail formation (see the spectrum labelled no RF in Fig. 17). The X-ray data have therefore conclusively demonstrated that the RF produces the energetic electron tail. It is true, however, that for somewhat lower plasma densities slide-away conditions exist. Photon spectra for these conditions are shown in Fig. 18.

---

†At very low densities the runaway current can make up the whole plasma current in a tokamak. The loop voltage becomes very small under these conditions and the electrons gain little energy in one transit around the machine. The photon-tail temperature becomes very small, and this plasma condition, therefore, is called slide-away regime.

The spectrum marked "without RF" that represents a typical slide-away spectrum tends to have a somewhat higher tail temperature than the spectrum generated by the RF.

Radial profiles of the X-ray tails during the RF pulse have been obtained with the Si(Li) detector system. Figure 19 plots the X-ray emission intensity at 14 keV, labelled S(14), versus the plasma radius. The data were obtained from straight line fits to photon tails as shown, for example, in Fig. 16B, and then Abel inverted. The figure shows that the formation of the energetic tails takes place in the central region of the plasma.

During the RF pulse, the energetic electrons have to carry practically the total plasma current, because the loop voltage vanishes. The radial X-ray profile should consequently also contain information on the location of the currents in the plasma. An exact evaluation of the current from X-ray profiles requires a large data base: the energy distribution in the tail has to be known as a function of radius. Also some data are needed on the ratio of parallel to perpendicular energy. These data are not available at present. Therefore, for a very first and preliminary estimate, we have made the assumption that the X-ray intensity will be proportional to the number of energetic electrons. If, in addition, their average velocity does not vary significantly with radius, then it is not unreasonable to assume that the X-ray profiles shown in Fig. 19 represent current density profiles.

The profile labelled A in Fig. 19 corresponds to normal current drive operation on PLT with a toroidal magnetic field B = 31 kG and a plasma current I_p = 200 kA. The X-ray profile (A) and presumably also the current profile seems very peaked. However, the safety factor q at the limiter is 10 for this discharge because of the plasma current was very small. Under these circumstances a regular ohmic-heating current profile would also be very

peaked. When the toroidal magnetic field is decreased (curve B) and when the plasma current is increased (curve C), the X-ray profiles consecutively broaden. Again, a regular discharge would show exactly the same behavior. By equating the X-ray profile with the current profile, a q-profile can be calculated. The resulting q for curves A, B, and C varies from slightly under 1 in the plasma center to 3-10 at the plasma edge. It was also observed that the X-ray profile, once it was established after the first 30 ms of current drive, remained unchanged for the rest of the RF pulse.

The creation of energetic electrons seems to produce a plasma of high conductivity in which the current profile seems to be frozen in. This finding from the X-ray data is in agreement with the fact that $\Lambda = \beta_\theta + \ell_i/2$ changes only slightly during LH current drive (Fig. 15). The X-ray data of Fig. 19 imply $\ell_i/2 = 0.9$, 0.7, and 0.6 for curves A, B, and C; values of Λ equal to 1.0, 0.8, and 0.6 were inferred from magnetic measurements with Mirnov coils.

The energy in the electron tail is approximately comparable to the thermal plasma energy, which in turn is considerably smaller than the magnetic energy stored in the poloidal field at these low plasma densities. The replacement of the ohmic current by a tail current requires, therefore, less RF power than an actual increase of the current. Experiments in which the RF power is varied have shown that there exists saturation of the X-ray intensity with power. The saturation seems to occur slightly below the power level required to keep the plasma current constant. In Fig. 20 we compare the X-ray spectra measured at RF powers of 11 kW and 200 kW. The 11 kW RF power produces a spectrum with a much flatter slope than that obtained for the 200 kW case. The RF fields seem to create a diffusion in velocity space that favors the creation of modestly energetic electrons (100 keV) and eliminates very high energy electrons. The often dramatic reduction of limiter X rays

with the onset of the RF power[27] provided the first indication of this effect.

Another factor that influences the slope of the X-ray tails is the phasing of the waveguides of the Brambilla[28] grill. In Fig. 21 two X-ray spectra are shown which were measured with phase angles of -135° and -60°, respectively, between neighboring waveguides. The -60° phasing gave a flatter spectrum and also a more efficient current drive.[25] A possible explanation for this flattening is illustrated in Fig. 22. The figure shows computed wave spectra according to Brambilla theory[28] for propagation parallel to the magnetic field. The parameter of the curves is the phasing of the waveguides on PLT. The kinetic energy of electrons that can resonate with the wave at the phase velocity, is indicated by the energy scale on the top right hand side. According to Fig. 22, the LH waves have a much higher phase velocity for 60° phasing than for the 135° phasing. A comparison of the energy of the resonant electrons and the electron tail temperature obtained in Fig. 17, shows that they are of comparable magnitude. The agreement is, however, not very quantitative. There is, for instance, a large gap in the 60° wave spectrum between 10 keV and 50 keV and it is not clear how electrons can be accelerated from the thermal part of the distribution through this gap into the tail. Nevertheless, we speculate a little bit further. Quasilinear theory would predict that $f(p) = \text{const}$ in a strong RF field (nonrelativistically $f(v) = \text{const}$). On the other hand, it was shown in Fig. 17 that the X-ray spectra can also be described by a free-fall distribution $f(p) = \text{const}$. What we might be seeing with the X-ray spectra is just the distribution function $f(p) = \text{const}$ with boundaries (E^*) determined by the wave spectrum (Fig. 22). It is clear that considerably more work has to be done to find out the true shape of the electron distribution function. In particular, it seems necessary to measure the X-ray emission as a function of

angle with respect to the magnetic field in order to find out whether the interpretation $f(p) = \text{const}$ is really tenable.

ACKNOWLEDGMENT

This work was supported by U.S. Department of Energy Contract No. DE-AC02-76-CHO-3073.

REFERENCES

[1] W. Stodiek, in Proceedings of the Fifth European Conference on Controlled Fusion and Plasma Physics, Grenoble, 1972, Vol. II, p.1.

[2] W. Hooke et al., Bull. Am. Phys. Soc. 26, 974-975 (1981).

[3] R. Dandl et al., Nucl. Fusion 4, 344 (1964).

[4] England and G. Haste, Phys. Rev. A 7, 383 (1973); Phys. Rev. A 8, 1475 (1973).

[5] J.L. Shohet and D. Greene, Phys. Rev. Lett. 27, 90 (1971).

[6] H. Knoepfel, in Diagnostics for Fusion Experiments, edited by P. Sindoni and C. Wharton (Pergamon Pres , New York, 1978).

[7] R.D. Evans, The Atomic Nucleus, (McGraw-Hill, New York, 1955).

[8] P. Brussard and M. van de Hulst, Rev. Mod. Phys. 34, 507 (1962).

[9] W. Heitler, The Quantum Theory of Radiation, (Oxford University Press, New York, 1954).

[10] M.W. Koch and J.W. Motz, Rev. Mod. Phys. 31, 920 (1959).

[11] R.H. Pratt, in Inner Shell and X-ray Physics of Atoms and Solids, edited by D. Fabian, H. Kleinpoppen, and C. Watson (Plenum Press, New York, 1981).

[12] H. Massey, E. Burhop, and H. Gilbody, Electronic and Ionic Impact Phenomena, (Oxford University Press, New York, 1969) Vol. II.

[13] H. L. Glucksstern and M. Hull, Phys. Rev. 90, 1030 (1953).

[14] C. Fronsdal and H. Überall, Phys. Rev. 111, 580, (1958).

[15] K. Bernhardi, Ph.D thesis, University Bochum, Germany, 1980.

[16] D. Hillis, Oak Ridge National Laboratory Report No. ORNL/TM-8179, 1982.

[17] D. ter Haar, Elements of Statistical Mechanics, (Holt, Rinehart, and Winston, New York, 1954).

[18] H. Zehrfeld, G. Fussmann, and B. Green, Plasma Phys. 23, 473 (1981).

[19]S. von Goeler and W. Stodiek, in Proceedings of the Fifth European Conference on Controlled Fusion and Plasma Physics, Grenoble, 1972, Vol. I, p. 2.

[20]S. von Goeler et al., in Proceedings of the Third International Symposium on Toroidal Plasma Confinement, Garching, 1973, paper B25.

[21]H. Dreicer, Phys. Rev. 117, 329 (1960).

[22]M. Kruskal and I. Bernstein, Princeton Plasma Physics Laboratory Report No. MATT-Q-20, 174 (1962).

[23]R. Kulsrud et al., Phys. Rev. Lett. 31, 690 (1973).

[24]S. Bernabei et al., Phys. Rev. Lett. 49, 1255 (1982).

[25]J. Stevens et al., in Proceedings of the Third Joint Varenna-Grenoble Conference On Heating in Toroidal Plasmas, 1982 Vol. 2, p. 455.

[26]F. Jobes et al., Physica Scri., T2, 418 (1982).

[27]I. Strachan (private communication).

[28]M. Brambilla, Nucl. Fusion 16, 47 (1976).

FIGURE CAPTIONS

FIG. 1 X-ray spectra from the ST tokamak, showing thermal spectra at low photon energies and superthermal tails at high energies. The parameter is the neutral gas filling pressure. For simplicity, only the continuum radiation has been plotted and line radiation has been omitted.

FIG. 2 Physical layout of the hard X-ray detector for plasma bremsstrahlung on PLT.

FIG. 3 Bremsstrahlung spectrum $k \cdot d\sigma/dk$ emitted by a single electron with kinetic energy T. k is the photon energy, $\bar{\sigma} = Z^2 r_o^2/137 = Z^2 e^6 m_o^{-2} c^{-5} \hbar^{-1}$ and $E_o = m_o c^2$. The dashed lines represent Born approximation results.[9] The dashed-dotted curve is for aluminum ions and approximates exact quantum mechanical results by the Elwert factor.[9] The dashed line for 60 keV holds for protons.

FIG. 4 Polarization of Bremsstrahlung.[12] Emission of the photons is at 90° with respect to the electron velocity. The curve is calculated for an electron energy $T_o/eV = 534Z^2$.

FIG. 5 Forward scattering of Bremsstrahlung.[12] Angular distribution of X-ray photons near the high frequency limit for 20 keV electrons on a thin magnesium target.

FIG. 6 X-ray spectra emitted by a beam of electrons (θ_e = 0.6°) with a relativistic Maxwellian energy distribution (Eq. 2) using a cross section derived by Gluckstern and Hull.[13] Detector-beam angle θ_d equals 90°. The electron tail temperature T is varied from 12.5 keV to 200 keV.

FIG. 7 Polarization of bremsstrahlung from an electron beam. Plotted is the ratio of the X-ray intensities polarized with the electric field vector perpendicular and parallel to the beam direction. Otherwise the data are the same as in Fig. 6.

FIG. 8 Bremsstrahlung from a 100 keV electron tail showing the effect of varying the electron cone angle θ_e. The detector-beam angle θ_d equals 90°. The density of tail electrons is the same for the three cases.

FIG. 9 Bremsstrahlung from a beam of electrons with a free-fall distribution f(p) = const (Eq. 8). Emission is at an angle of 60° for subfigure(a) and at an angle of 3° for subfigure (b). The parameter E* (Eq. 9) is given in units of m_0c^2 = 511 keV.

FIG. 10 Radial distribution of hard X-ray photons from ST.

FIG. 11 X-ray spectra from runaway electrons measured at an angle of ± 30° with respect to the major radius on ST. The theoretical curves represent spectra calculated with the free-fall distribution f(p) = const.

FIG. 12 Comparison of a tangential spectrum with a 60° spectrum from ST. The solid curves represent free-fall spectra at 3° and 60°. The dashed curve represents the 60° free-fall spectrum divided by a factor of 8 to account for the reduction in line of sight.

FIG. 13 A time sequence of three X-ray spectra is shown in subfigure (a) and (b) for two ST discharges. A free-fall spectrum is fitted to the spectrum measured at 14 ms, and the expected free-fall spectra for t = 27 ms and 40 ms are plotted. The graph on the right shows the runaway-electron confinement time τ_{Re} deduced from final stationary X-ray spectrum.

FIG. 14 Electron runaway rate vs. the electric field in terms of the critical electric field.[23] Various earlier theoretical predictions by Dreicer,[21] Gurevich, Lebedev, and Kruskal and Bernstein[22] predict larger rates than the experimental observations (open circles). Kulsrud and Sun[23] succeeded in obtaining order of magnitude agreement by including the effect of impurities and also the effects of finite electron confinement. The confinement time τ seems, however, somewhat shorter than the one shown in Fig. 13.

FIG. 15 Typical discharge with lower-hybrid current drive, showing plasma current, RF power, loop voltage, average plasma density and $\Lambda = \beta_\theta + \ell_i/2 = R_i/2$ versus time.

FIG. 16 Typical X-ray spectra measured (A) before and (B) during current drive with a Si(Li) detector. A straight line fit to the spectrum

in subfigure (B) from 14 keV to 25 keV indicates a photon tail temperature of 29 keV.

FIG. 17 X-Ray spectrum with and without current drive at a plasma density of 6×10^{12} cm^{-3}. The solid curves represent calculated X-ray spectra for a beam of electrons (θ_e = 0.6°) having either a Maxwellian distribution with a tail temperature of T = 150 keV or a free-fall distribution with E^* = 600 keV.

FIG. 18 X-ray spectrum with and without current drive at a plasma density of 3×10^{12} cm^{-3}. The open circles represent a typical slide-away spectrum.

FIG. 19 Radial profiles of the X-ray emission. Plotted is the Abel inverted X-ray intensity at 14 keV photon energy versus radius measured with the Si(Li) detector on PLT. Profile (A) is with B = 31 kG and I_p = 200 kA, profile (B) with B = 16 kG and I_p = 210 kA and (C) with B = 15 kG and I_p = 290 kA.

FIG. 20 Hard X-ray spectra for an RF power level of 11 kW and 200 kW. (Phasing is -90°).

FIG. 21 Hard X-ray spectra for two different phasings (-60° and -135°) of the Brambilla grill on PLT.

FIG. 22 RF Power spectrum for various phases of the Brambilla grill,[28] as calculated by S. Bernabei.

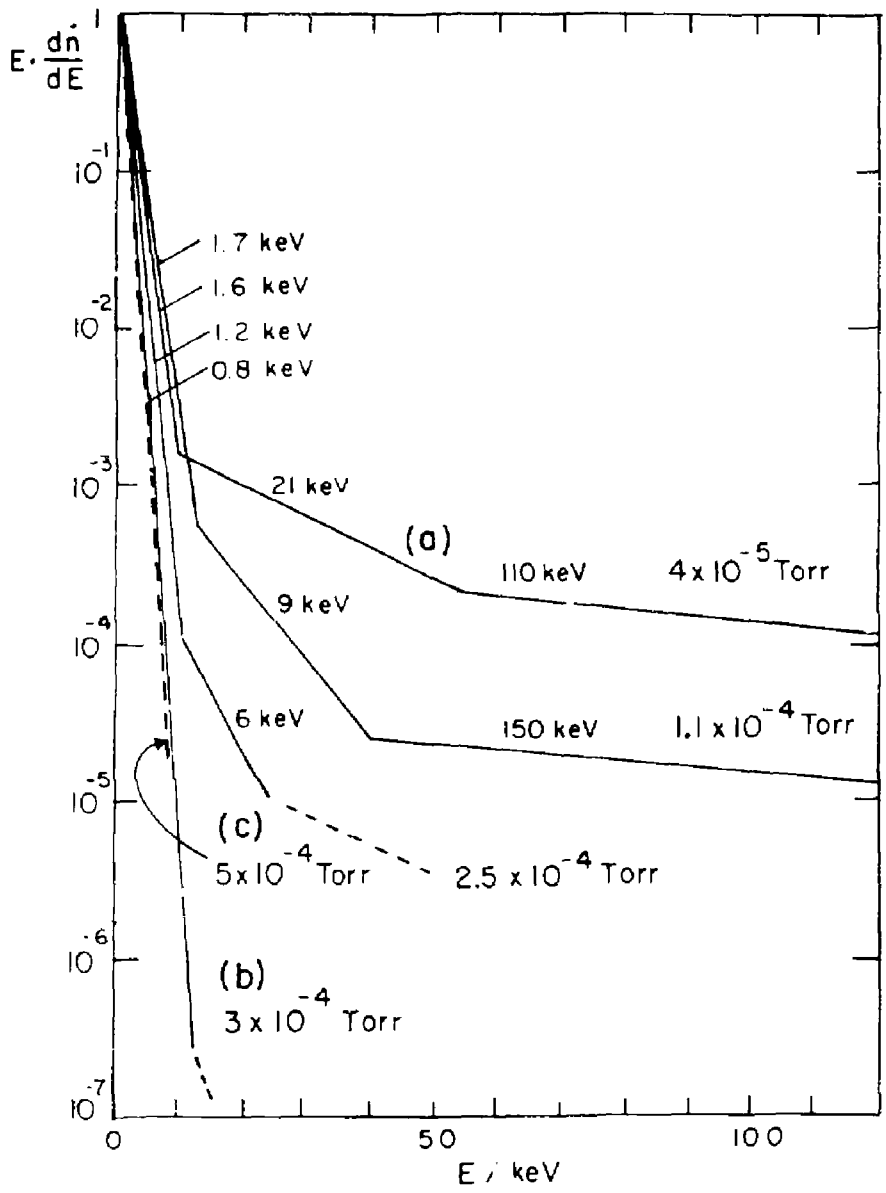
E · dn/dE
1
10^-1
10^-2
10^-3
10^-4
10^-5
10^-6
10^-7
1.7 keV
1.6 keV
1.2 keV
0.8 keV
21 keV
(a)
110 keV
4 x 10^-5 Torr
9 keV
6 keV
150 keV
1.1 x 10^-4 Torr
(c)
5 x 10^-4 Torr
2.5 x 10^-4 Torr
(b)
3 x 10^-4 Torr
0
50
100
E / keV

Fig. 1

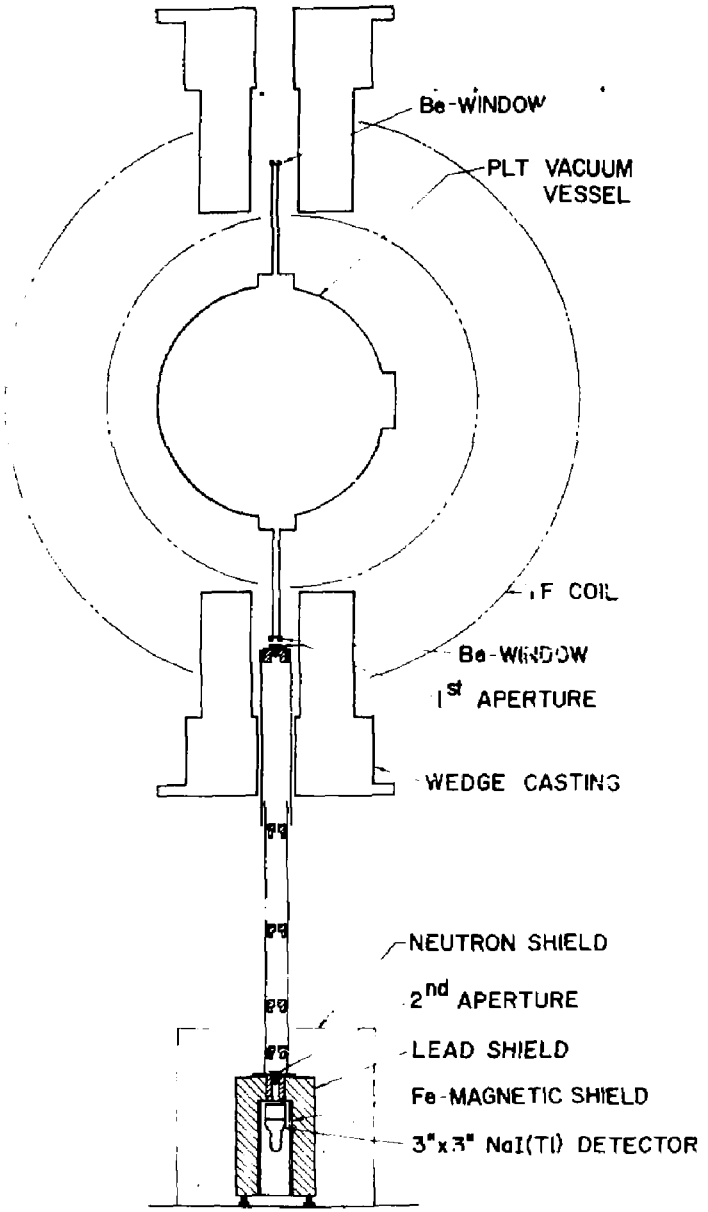
Be-WINDOW
PLT VACUUM VESSEL
TF COIL
Be-WINDOW
1st APERTURE
WEDGE CASTING
NEUTRON SHIELD
2nd APERTURE
LEAD SHIELD
Fe-MAGNETIC SHIELD
3"x3" NaI(Tl) DETECTOR

Fig. 2

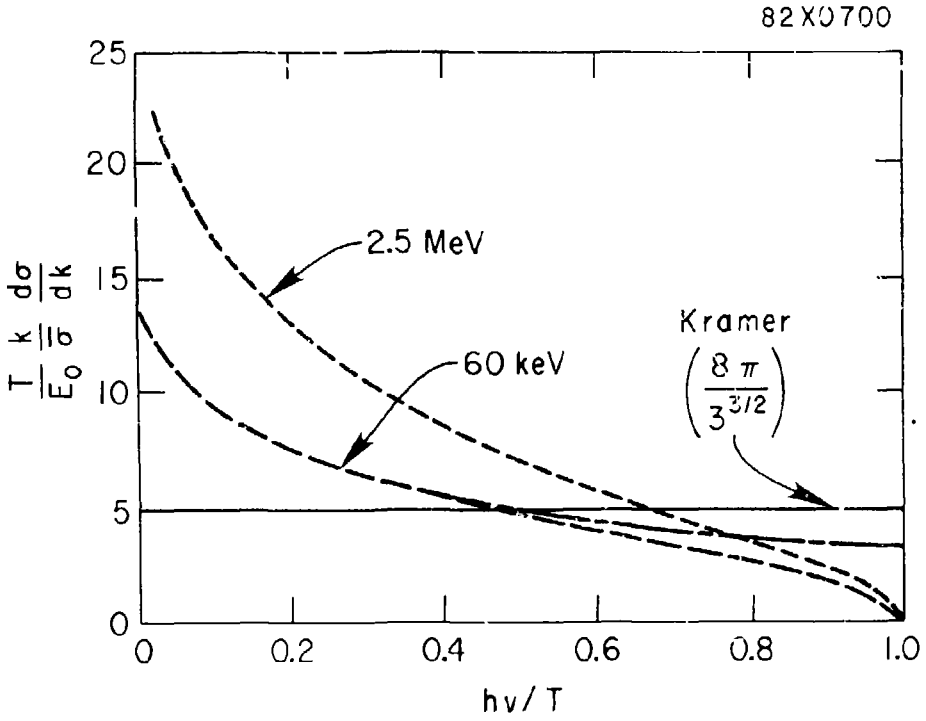
82X0700
25
20
15
10
5
0
0
0.2
0.4
0.6
0.8
1.0
hv/T
$\frac{T}{E_0}\frac{k}{\sigma}\frac{d\sigma}{dk}$
2.5 MeV
60 keV
Kramer
$\left(\frac{8\pi}{3^{3/2}}\right)$

Fig. 3

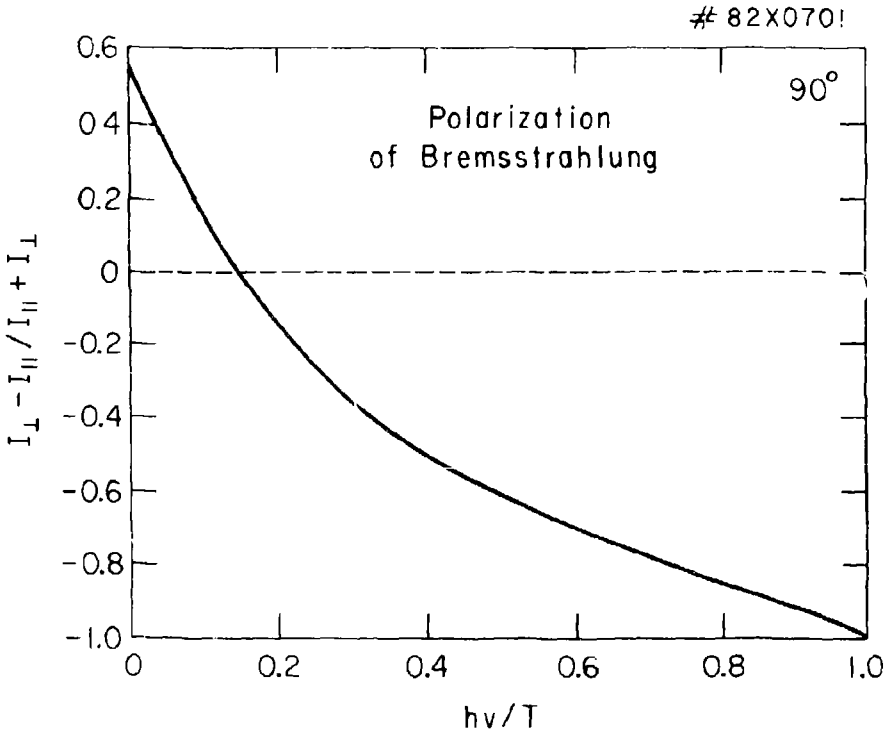
#82X0701
90°
Polarization
of Bremsstrahlung
0.6
0.4
0.2
0
-0.2
-0.4
-0.6
-0.8
-1.0
0
0.2
0.4
0.6
0.8
1.0
hv/T
$I_\perp - I_\parallel / I_\parallel + I_\perp$

Fig. 4

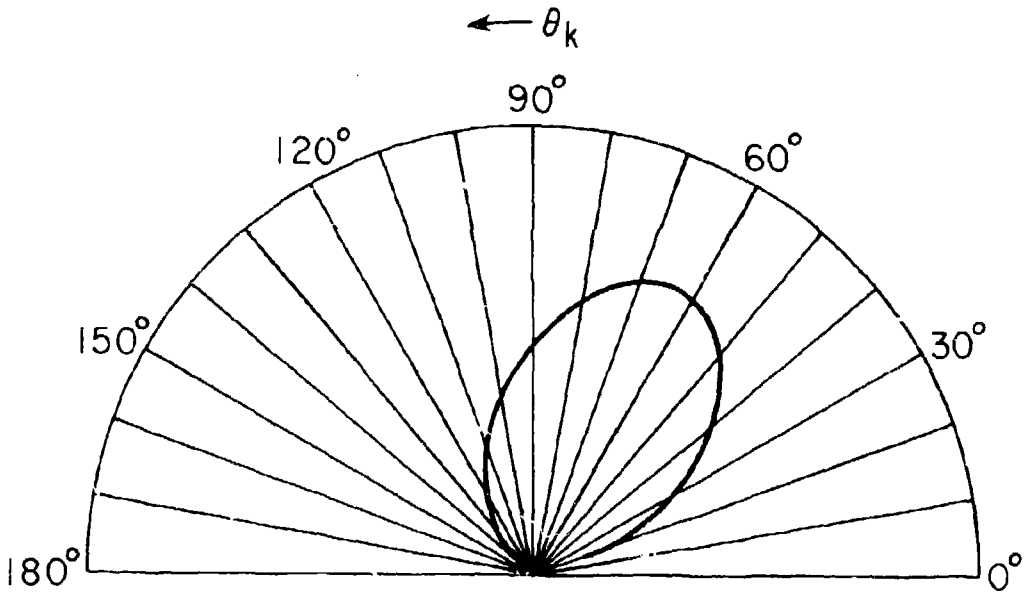

Fig. 5

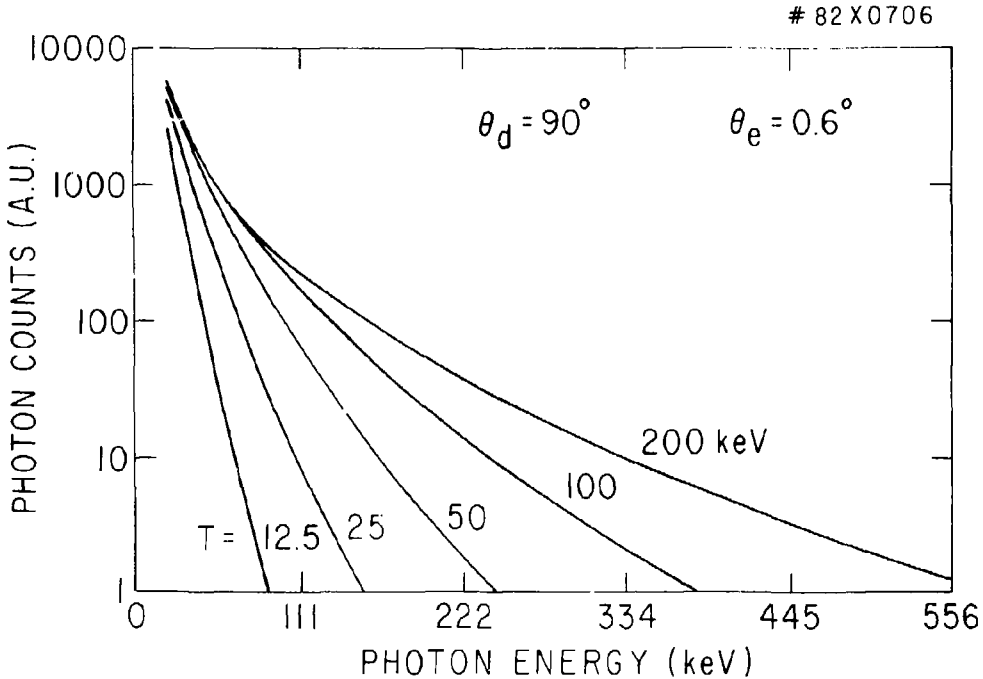
82X0706
10000
1000
100
10
1
PHOTON COUNTS (A.U.)
$\theta_d = 90°$
$\theta_e = 0.6°$
200 keV
100
50
25
12.5
T =
0
111
222
334
445
556
PHOTON ENERGY (keV)

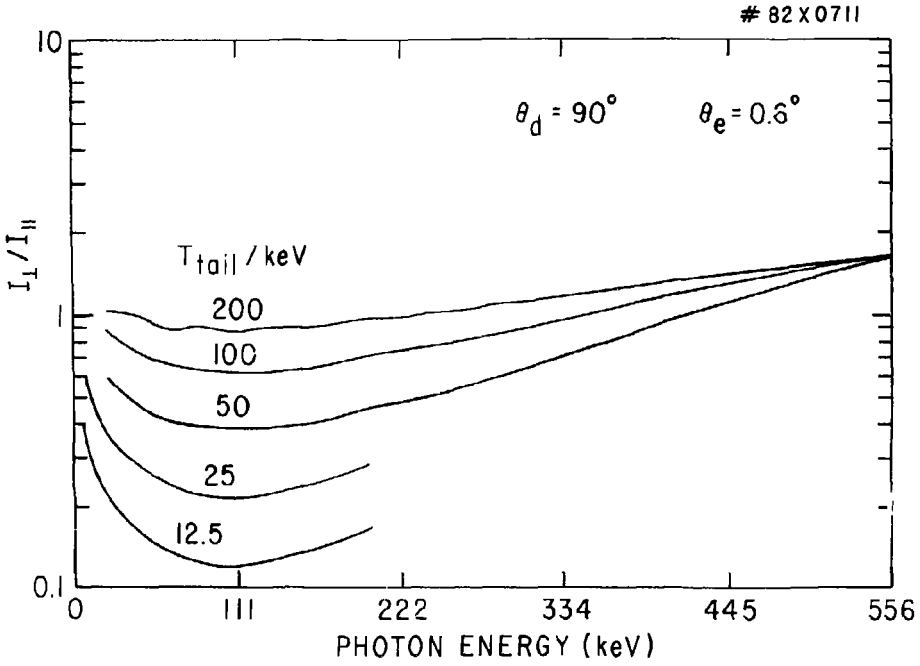
82X0711
10
1
0.1
$\theta_d = 90°$
$\theta_e = 0.6°$
$I_\perp / I_\parallel$
T_{tail} / keV
200
100
50
25
12.5
0
111
222
334
445
556
PHOTON ENERGY (keV)

Fig. 7

82 X 0714

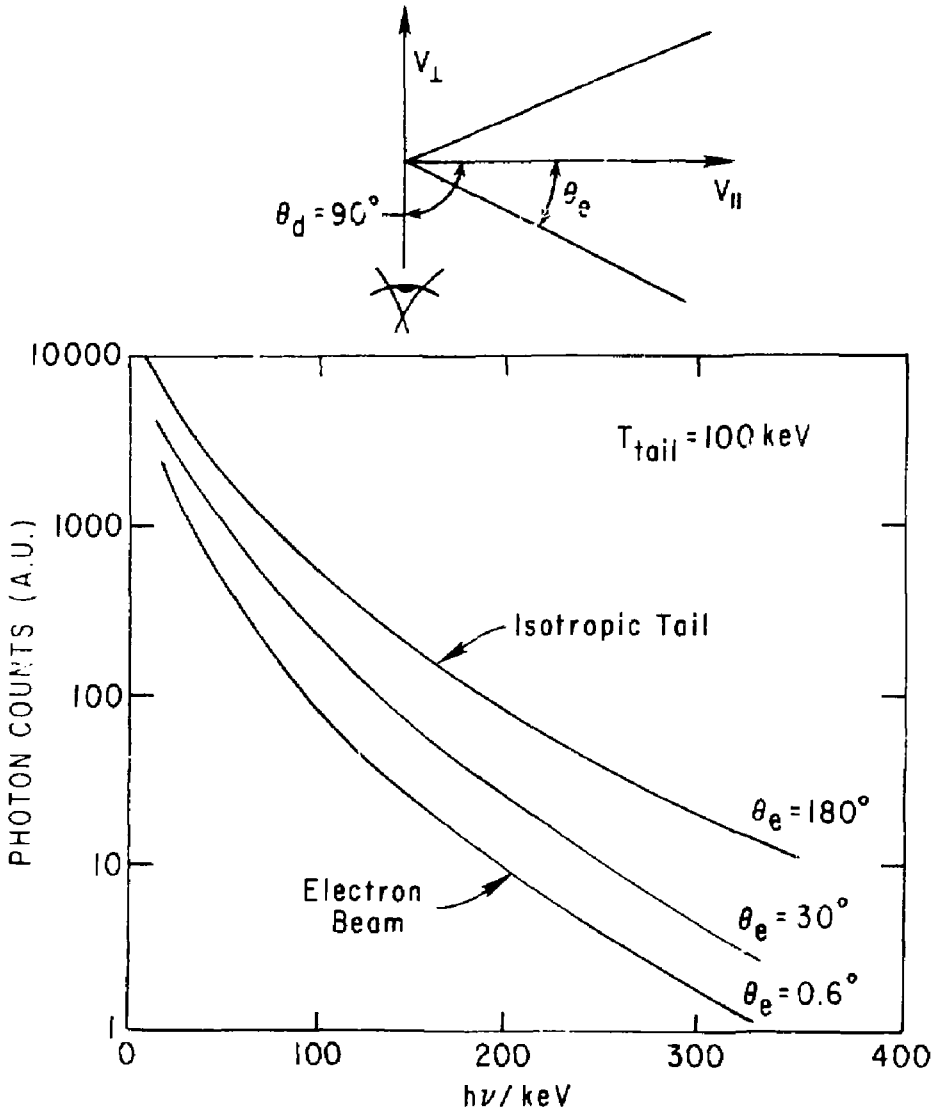

Fig. 8

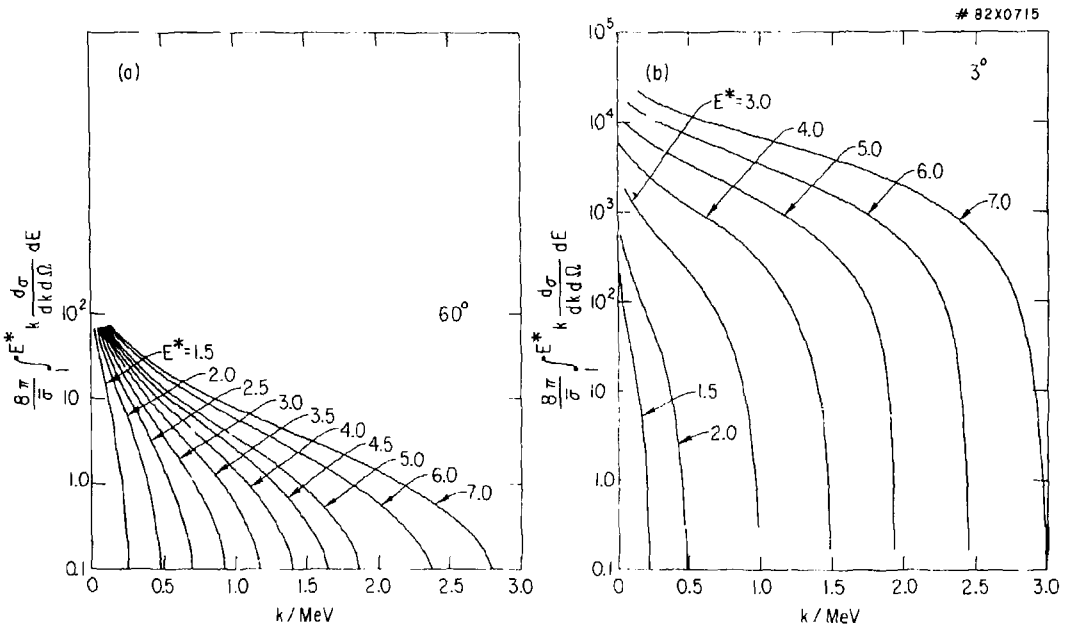
#82X0715
(a)
60°
E*=1.5
2.0
2.5
3.0
3.5
4.0
4.5
5.0
6.0
7.0
(b)
3°
E*=3.0
4.0
5.0
6.0
7.0
1.5
2.0
k / MeV

Fig. 9

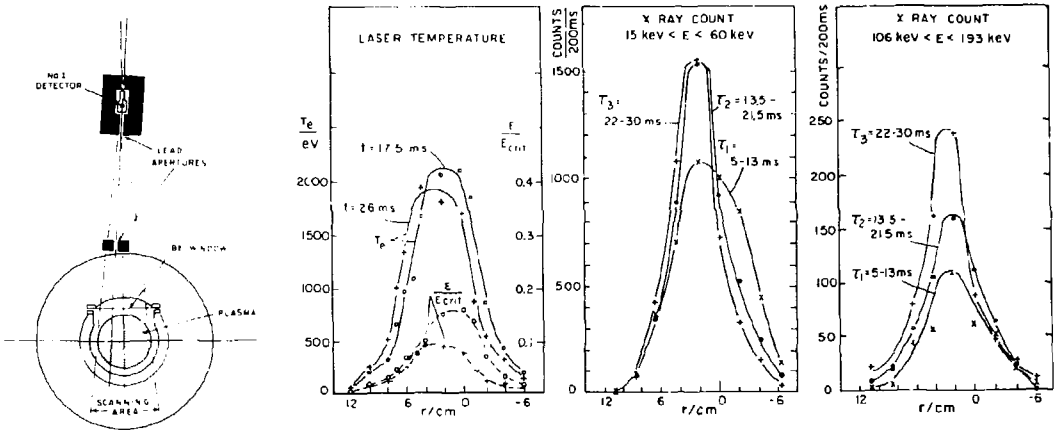
NaI DETECTOR
LEAD APERTURES
BF WINDOW
PLASMA
SCANNING AREA
LASER TEMPERATURE
T_e eV
$\frac{E}{E_{crit}}$
t = 17.5 ms
t = 26 ms
T_e
$\frac{E}{E_{crit}}$
r/cm
X RAY COUNT
15 kev < E < 60 kev
COUNTS/200ms
T_3 = 22-30 ms
T_2 = 13.5 - 21.5 ms
T_1 = 5-13 ms
r/cm
X RAY COUNT
106 kev < E < 193 kev
COUNTS/200ms
T_3 = 22-30 ms
T_2 = 13.5 - 21.5 ms
T_1 = 5-13 ms
r/cm

Fig. 13

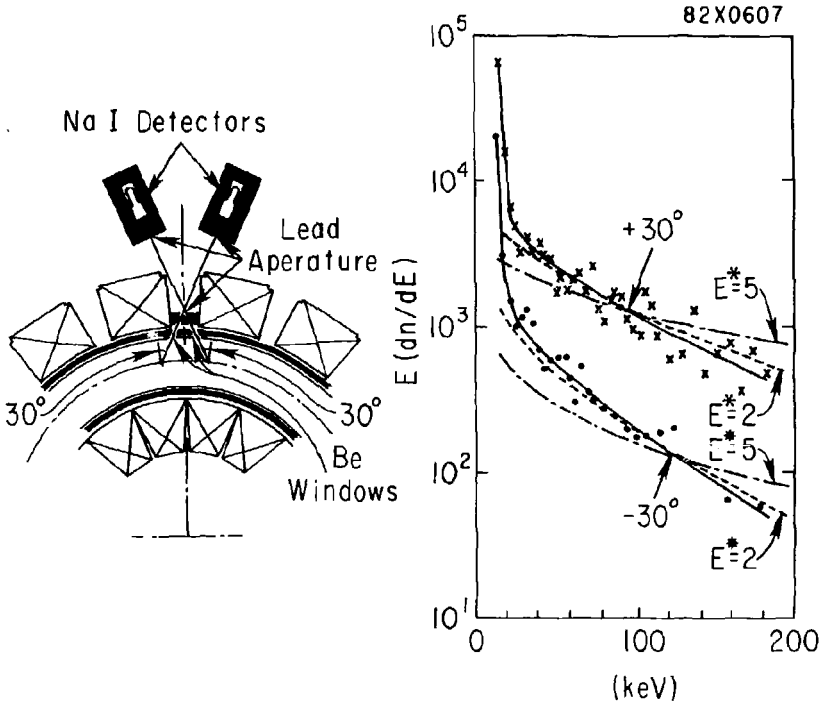
Na I Detectors
Lead
Aperature
30°
30°
Be
Windows
82X0607
10^5
10^4
10^3
10^2
10^1
E (dn/dE)
+30°
E*=5
E*=2
E*=5
-30°
E*=2
0
100
200
(keV)

Fig. 11

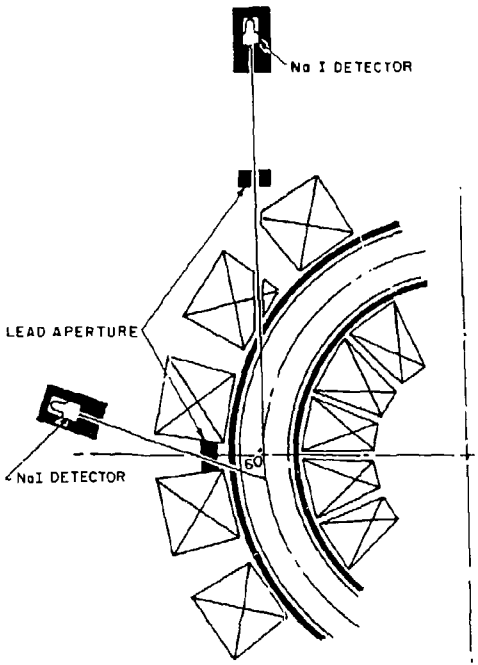
Na I DETECTOR
LEAD APERTURE
NaI DETECTOR
60°

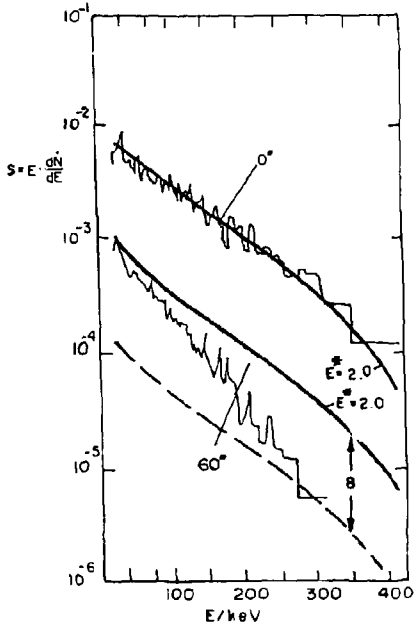
$S = E \cdot \frac{dN}{dE}$
10^{-1}
10^{-2}
10^{-3}
10^{-4}
10^{-5}
10^{-6}
0°
60°
E = 2.0
E = 2.0
8
100
200
300
400
E/keV

Fig. 1.

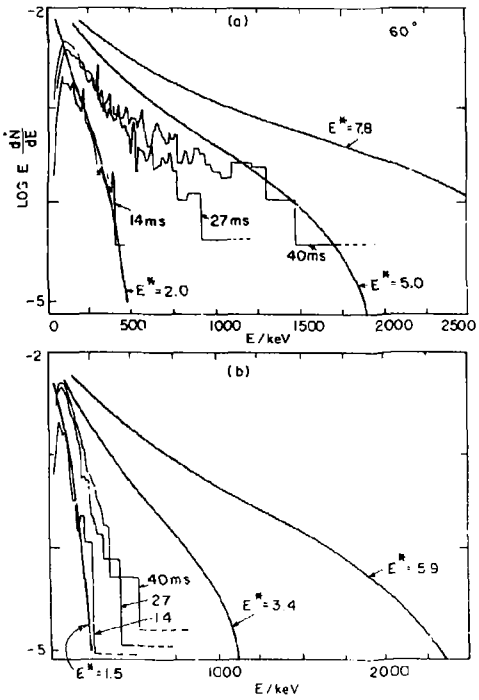
(a)
60°
$E^* = 7.8$
14ms
27ms
40ms
$E^* = 2.0$
$E^* = 5.0$
$\log E \frac{dN}{dE}$
E / keV
(b)
40ms
27
14
$E^* = 5.9$
$E^* = 3.4$
$E^* = 1.5$
E / keV

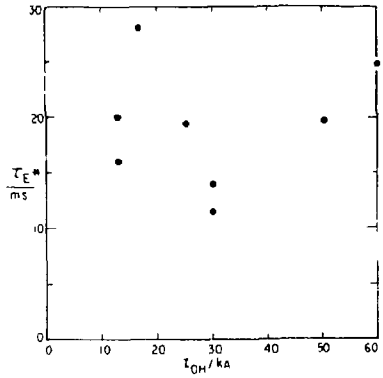
$\frac{\tau_{E^*}}{ms}$
I_{OH} / kA

Fig. 13

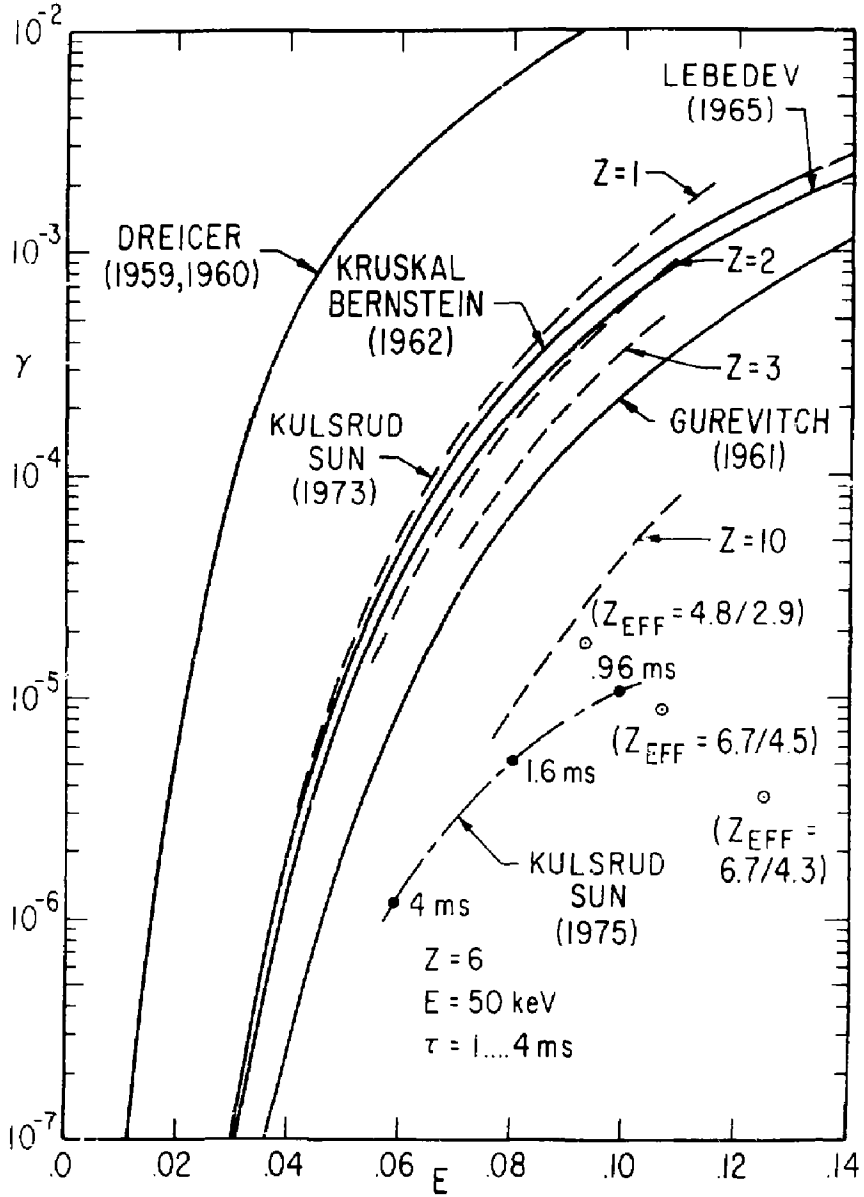
LEBEDEV
(1965)
Z=1
DREICER
(1959,1960)
KRUSKAL
BERNSTEIN
(1962)
Z=2
Z=3
KULSRUD
SUN
(1973)
GUREVITCH
(1961)
Z=10
(Z_EFF=4.8/2.9)
.96 ms
(Z_EFF=6.7/4.5)
1.6 ms
(Z_EFF=
6.7/4.3)
KULSRUD
SUN
(1975)
4 ms
Z=6
E=50 keV
τ=1....4 ms
γ
E
10^-2
10^-3
10^-4
10^-5
10^-6
10^-7
.0
.02
.04
.06
.08
.10
.12
.14

Fig. 14

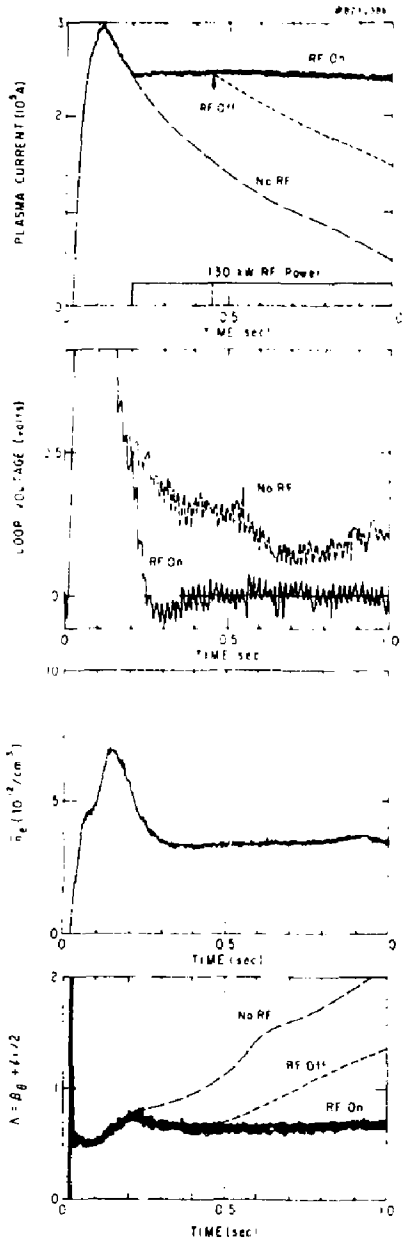
PLASMA CURRENT (10^3 A)
RF On
RF Off
No RF
130 kW RF Power
TIME sec
LOOP VOLTAGE (volts)
No RF
RF On
TIME sec
n_e (10^-2/cm^3)
TIME (sec)
Λ = β_θ + ℓ_i/2
No RF
RF Off
RF On
TIME (sec)

Fig. 15

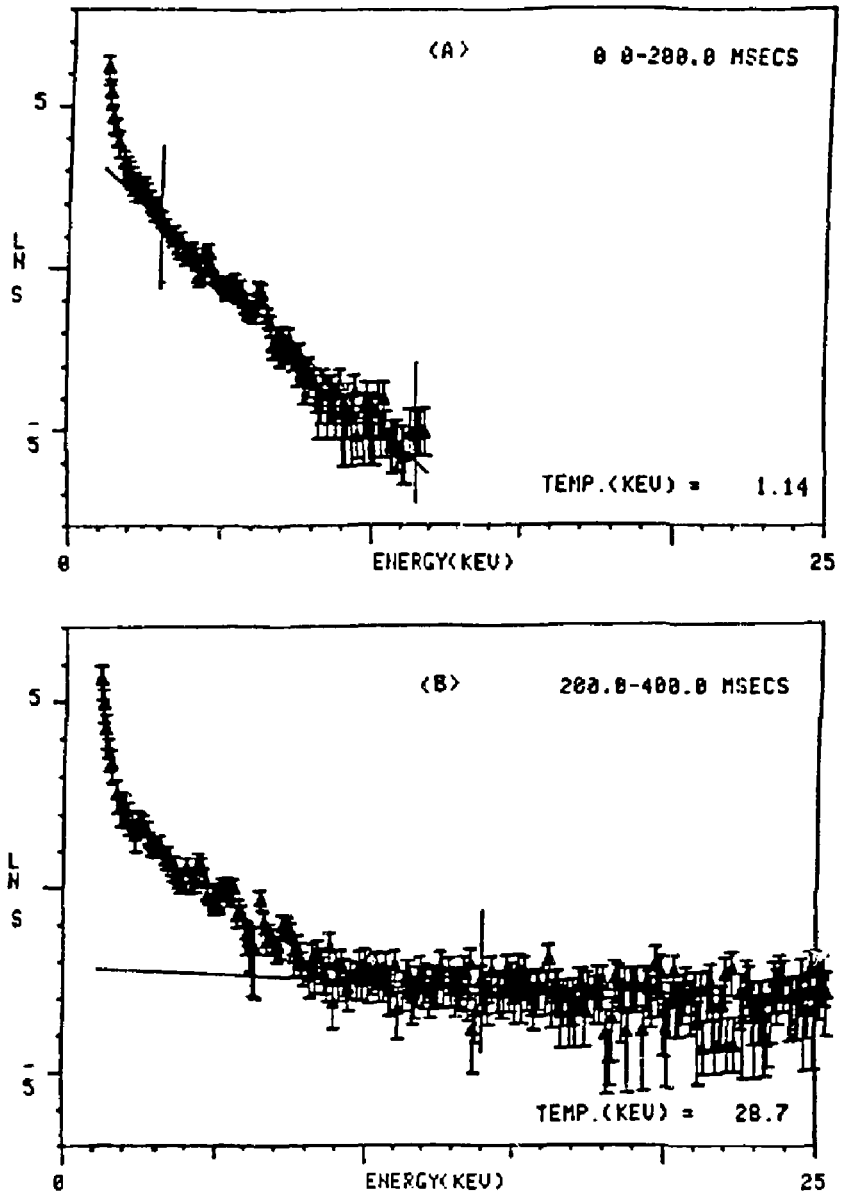
(A)
0 0-200.0 MSECS
TEMP.(KEV) = 1.14
ENERGY(KEV)
0
25
(B)
200.0-400.0 MSECS
TEMP.(KEV) = 28.7
ENERGY(KEV)
0
25

Fig. 16

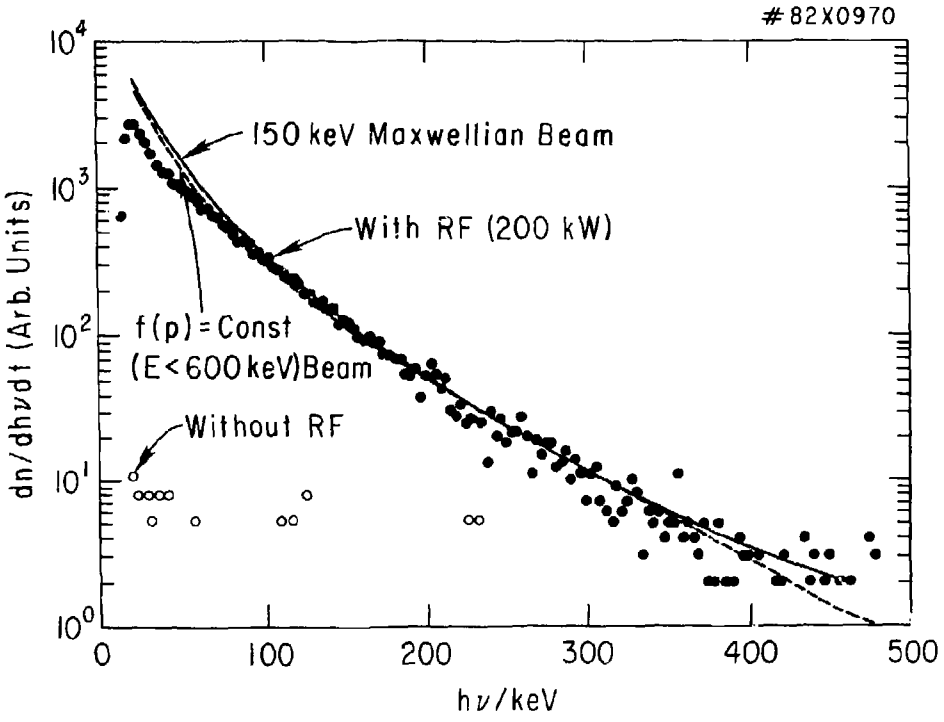
#82X0970
150 keV Maxwellian Beam
With RF (200 kW)
f(p) = Const
(E < 600 keV) Beam
Without RF
dn/dhνdt (Arb. Units)
hν/keV
10^4
10^3
10^2
10^1
10^0
0
100
200
300
400
500

Fig. 17

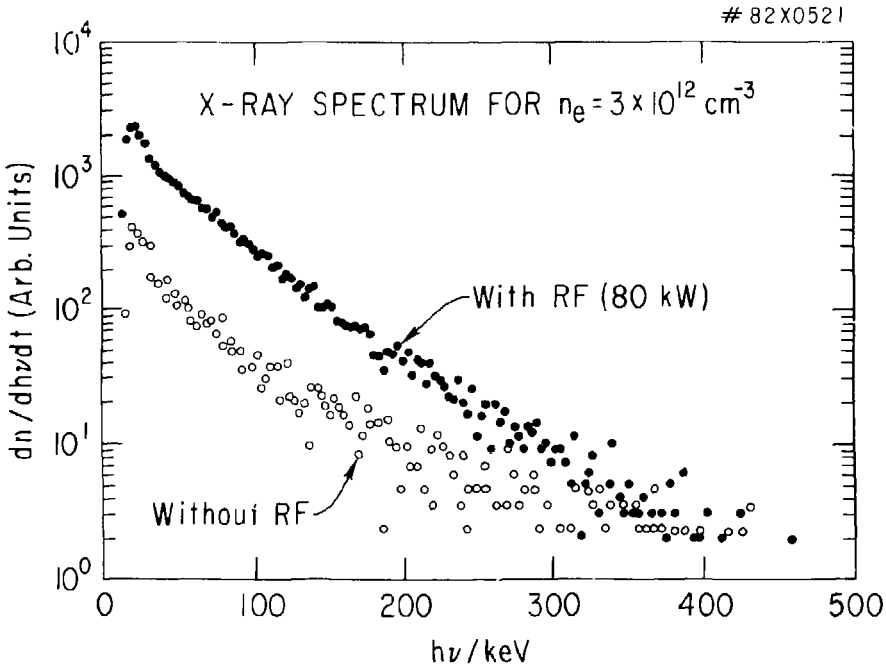
#82X0521
X-RAY SPECTRUM FOR $n_e = 3 \times 10^{12}$ cm^{-3}
With RF (80 kW)
Without RF
dn/dhνdt (Arb. Units)
hν/keV
10^4
10^3
10^2
10^1
10^0
0
100
200
300
400
500

Fig. 15

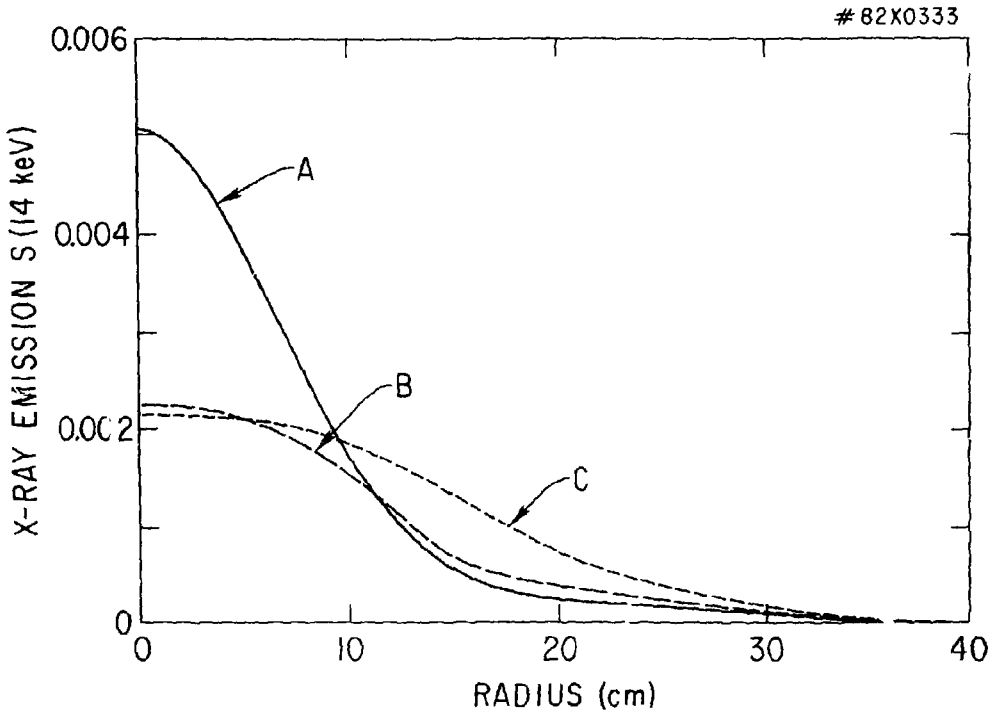
#82X0333
0.006
0.004
0.002
0
X-RAY EMISSION S(14 keV)
A
B
C
0
10
20
30
40
RADIUS (cm)

Fig. 19

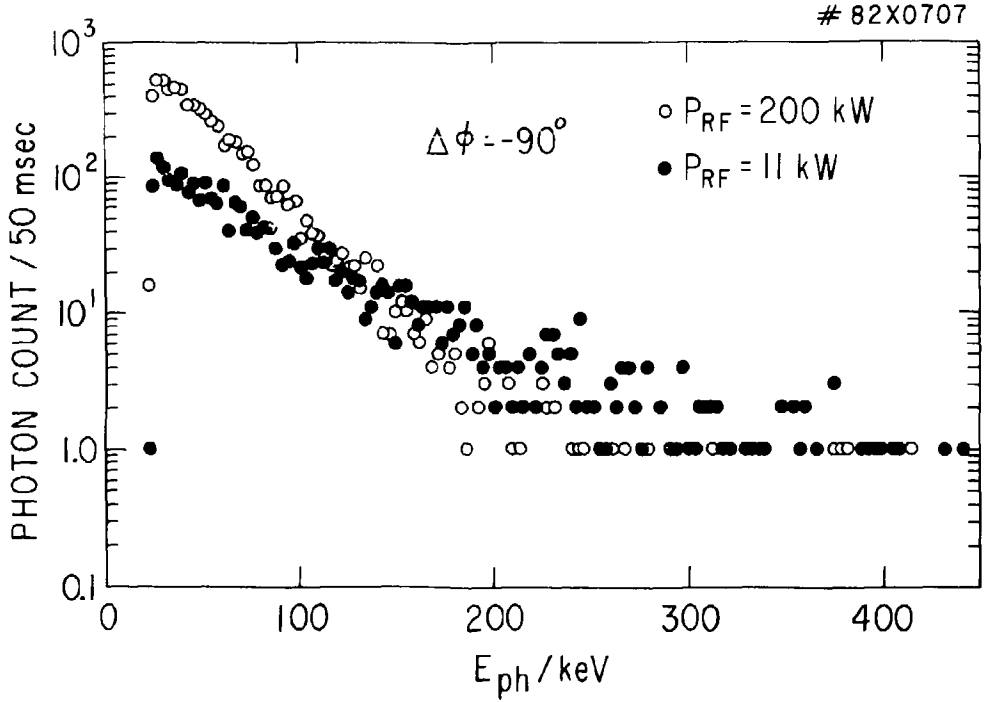
82X0707
PHOTON COUNT / 50 msec
10^3
10^2
10^1
1.0
0.1
0
100
200
300
400
E_{ph} / keV
$\Delta\phi = -90^\circ$
P_{RF} = 200 kW
P_{RF} = 11 kW

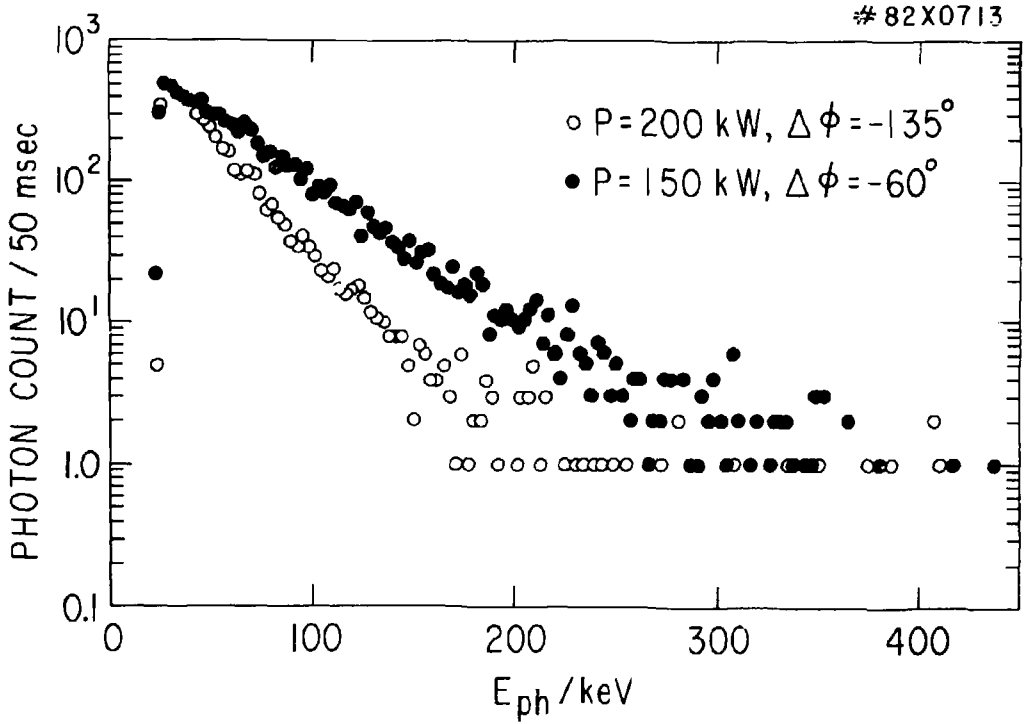
#82X0713
PHOTON COUNT / 50 msec
10^3
10^2
10^1
1.0
0.1
0
100
200
300
400
E_{ph} / keV
○ P = 200 kW, Δφ = -135°
● P = 150 kW, Δφ = -60°

Fig. 21

#82X0703

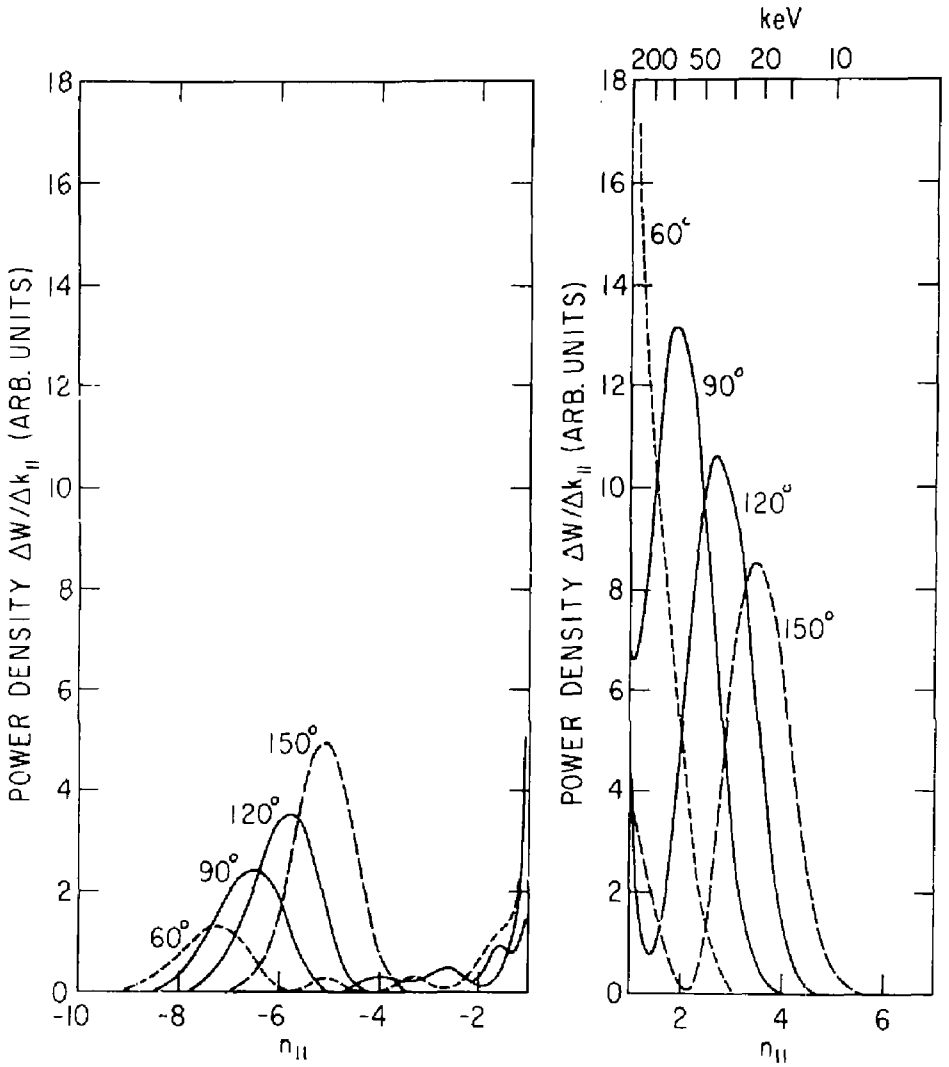

Fig. 22

EXTERNAL DISTRIBUTION IN ADDITION TO TIC UC-20

Plasma Res Lab, Austra Nat'l Univ, AUSTRALIA
Dr. Frank J. Paoloni, Univ of Wollongong, AUSTRALIA
Prof. I.R. Jones, Flinders Univ., AUSTRALIA
Prof. M.H. Brennan, Univ Sydney, AUSTRALIA
Prof. F. Cap, Inst Theo Phys, AUSTRIA
Prof. Frank Verheest, Inst theoretische, BELGIUM
Dr. D. Palumbo, Dc XII Fusion Prog, BELGIUM
Eco e Royale Militaire, Lab de Phys Plasmas, BELGIUM
Dr. P.H. Sakanaka, Univ Estadual, BRAZIL
Dr. C.R. James, Univ of Alberta, CANADA
Prof. J. Teichmann, Univ of Montreal, CANADA
Dr. A.V. Sharsard, Univ of Saskatchewan, CANADA
Prof. S.R. Sreenivasan, University of Calgary, CANADA
Prof. Tudor W. Johnston, INRS-Energie, CANADA
Dr. Hannes Barnard, Univ British Columbia, CANADA
Dr. M.P. Bachynski, MPB Technologies, Inc., CANADA
Zhengwu Li, SW Inst Physics, CHINA
Library, Tsing Hua University, CHINA
Librarian, Institute of Physics, CHINA
Inst Plasma Phys, SW Inst Physics, CHINA
Dr. Peter Lukac, Komenskeho Univ, CZECHOSLOVAKIA
The Librarian, Culham Laboratory, ENGLAND
Prof. Schatzman, Observatoire de Nice, FRANCE
J. Radet, CEN-BP6, FRANCE
AM Dupas Library, AM Dupas Library, FRANCE
Dr. Tom Mual, Academy Bibliographic, HONG KONG
Preprint Library, Cent Res Inst Phys, HUNGARY
Dr. A.K. Sundaram, Physical Research Lab, INDIA
Dr. S.K. Trehan, Panjab University, INDIA
Dr. Indra Mohan Lal Das, Banaras Hindu Univ, INDIA
Dr. L.K. Chavda, South Gujarat Univ, INDIA
Dr. R.K. Chhajlani, Var Ruchi Marg, INDIA
P. Kaw, Physical Research Lab, INDIA
Dr. Phillip Rosenau, Israel Inst Tech, ISRAEL
Prof. S. Cuperman, Tel Aviv University, ISRAEL
Prof. G. Rostagni, Univ Di Padova, ITALY
Librarian, Int'l Ctr Theo Phys, ITALY
Miss Clelia De Palo, Assoc EURATOM-CNEN, ITALY
Biblioteca, del CNR EURATOM, ITALY
Dr. K. Yamato, Toshiba Res & Dev, JAPAN
Prof. M. Yoshikawa, JAERI, Tokai Res Est, JAPAN
Prof. T. Uchida, University of Tokyo, JAPAN
Research Info Center, Nagoya University, JAPAN
Prof. Kyoji Nishikawa, Univ of Hiroshima, JAPAN
Prof. Sigeru Mori, JAERI, JAPAN
Library, Kyoto University, JAPAN
Prof. Ichiro Kawakami, Nihon Univ, JAPAN
Prof. Satoshi Itoh, Kyushu University, JAPAN
Tech Info Division, Korea Atomic Energy, KOREA
Dr. R. England, Ciudad Universitaria, MEXICO
Bibliotheek, Fom-Inst Voor Plasma, NETHERLANDS
Prof. R.S. Lilley, University of Waikato, NEW ZEALAND
Dr. Suresh C. Sharma, Univ of Calabar, NIGERIA
Prof. J.A.C. Cabral, Inst Superior Tech, PORTUGAL
Dr. Octavian Petrus, ALI CUZA University, ROMANIA
Dr. R. Jones, Nat'l Univ Singapore, SINGAPORE
Prof. M.A. Hellberg, University of Natal, SO AFRICA
Dr. Johan de Villiers, Atomic Energy Bd, SO AFRICA
Dr. J.A. Tagle, JEN, SPAIN
Prof. Hans Wilhelmson, Chalmers Univ Tech, SWEDEN
Dr. Lennart Stenflo, University of UMEA, SWEDEN
Library, Royal Inst Tech, SWEDEN
Dr. Erik T. Karlson, Uppsala Universitet, SWEDEN
Centre de Recherchesen, Ecole Polytech Fed, SWITZERLAND
Dr. W.L. Weise, Nat'l Bur Stand, USA
Dr. W.M. Stacey, Georg Inst Tech, USA
Dr. S.T. Wu, Univ Alabama, USA
Prof. Norman L. Oleson, Univ S Florida, USA
Dr. Benjamin Ma, Iowa State Univ, USA
Prof. Magne Kristiansen, Texas Tech Univ, USA
Dr. Raymond Askew, Auburn Univ, USA
Dr. V.T. Tolok, Kharkov Phys Tech Ins, USSR
Dr. O.D. Ryutov, Siberian Acad Sci, USSR
Dr. M.S. Rabinovich, Lebedev Physical Inst, USSR
Dr. G.A. Eliseev, Kurchatov Institute, USSR
Dr. V.A. Glukhikh, Inst Electro-Physical, USSR
Prof. T.J. Boyd, Univ College N Wales, WALES
Dr. K. Schindler, Ruhr Universitat, W. GERMANY
Nuclear Res Estab, Julich Ltd, W. GERMANY
Librarian, Max-Planck Institut, W. GERMANY
Dr. H.J. Kaeppler, University Stuttgart, W. GERMANY
Bibliothek, Inst Plasmaforschung, W. GERMANY